Failure Mechanisms and Solutions for Fin-Pass Rolls Repair-Ring at an Electric Resistance Welding Pipe Plant

Mahammad Laribaghal[1*], Mehdi Torfi[2], Mehdi Khorasanian[2], and Seyyed Reza Alavi Zaree[2]

[1] Assistant Professor, Department of Materials Science and Engineering, Faculty of Engineering, Shahid Chamran University of Ahvaz, Ahvaz, 61357-83151, Iran
[2] Assistant Professor, Department of Materials Science and Engineering, Faculty of Engineering, Shahid Chamran University of Ahvaz, Ahvaz, 61357-83151, Iran

Highlights

- The repair of the fin-pass roller using repair rings and its failure mechanism are investigated;
- The stresses on fin-pass rollers are studied using the finite element simulation method;
- The optimization of repair ring materials and their wear behavior is studied.

Abstract

Fin-pass rolls are the latest series of rolls in electric resistance welding (ERW) pipe production lines that form the sheets to tubular shape and adjust the edges of the sheet for welding. The rolls (made of AISI 8622 steel) lose their proper function after about 10 years of operation due to severe wear and change of their original surface profile. The worn portions were removed by grinding and replaced by an AISI D2 high carbon steel ring to repair these rolls. After a short time of service (about one year), the edge of the repair ring was exposed to severe spalling and fracture. The present study investigated the causes of the rapid failure of the AISI D2 repair ring and proposed a solution to the problem. The surface morphology, hardness, and wear resistance were studied. Moreover, the stress analysis of fin-pass rolls was studied using ABAQUS 6.14 finite element software for the closer investigation of the failure mechanism. The leading cause of spalling was the inherent brittleness of the AISI D2 steel and the presence of a high-stress concentration at the edges of the repair ring. To overcome this problem, carburized AISI P20 steel, case hardened AISI 4140 steel, and hard chromium electroplated AISI 4140 steel were replaced, and the resulting properties were studied. The highest resistance to spalling and wear occurred with carburized AISI P20 steel because of the high surface hardness and the gradual increase of toughness from the surface to the depth in the carburizing process, increasing the wear resistance and retarding the growth of fatigue cracks.

Keywords: Carburizing; Failure mechanism; Finite element simulation; Fin-pass roller; Wear test.

* Corresponding author :
   Email: m.lari@scu.ac.ir

1. Introduction

In the cold roll forming process of pipes, a metal sheet is continuously deformed into a particular tubular shape through a series of rolls installed at the tandems along the longitudinal direction (Kasaei et al., 2014; Jiang et al., 2009). After forming a desired tubular shape, the edges of the sheet are joined by the electric resistance welding (ERW) process (Michitoshi, 2004). Pipes produced in this way are widely used in various industries such as oil, gas, and petrochemicals (William, 2011). In a series of rolls, the fin-pass rolls are responsible for accurately regulating the edges of the tubular-shaped product before welding (Yokoyama, 1981). The fin-pass roll has three sections, a fin roll and two fin side rolls (Kiuchi, 1986). The fin-side rolls are rotatable by a drive shaft, but the fin roll is rotatable freely and independent of the drive shaft (Yokoyama, 1981; Kiuchi, 1986). The fin-pass roll was subjected to considerable radial rolling and frictional forces arising from the contact between the roll and the steel tube, leading to severe working conditions for an extended period, which can destroy the cross-sectional profile of the side rolls due to wear and spalling of edges.

Many surface modification methods such as chromium plating, case hardening, and surface carburizing have been used to increase the lifetimes of the rolls (Budzakova, 2014; Cleiton, 2009; Fedrizzi, 2002; Klenk, 2003; Premsai, 2014). These repair processes usually enhance the surface's hardness and wear resistance. Understanding the forming process and the mechanical forces involved is essential for investigating the failure mechanisms of the rolls. Many studies investigated the forming process of pipe plants (Li, 2010; Kim, 2003; Jiang, 2009). However, the investigation on the forming stresses on the rolls is rear, which can help better understand the failure mechanisms of the rolls and better prevent premature failures. Studies have been done on the causes of the destruction of some forming rollers, such as rolling rollers. However, there are very few studies on the causes of fin-pass roller damage (Wu, 2008; Li, 2007a; Ray, 2000). Due to the high costs of the rolls, repairing processes are reasonably economic. Repairing the worn fin-pass roll is very important, and various processes are used to repair the rolls in the industry. Repair welding is employed for the Treiber rolls, and the repaired rolls are susceptible to cracking (Tanasković, 2017; Wang, 2018). In addition, repair welding can be expensive and time-consuming (Zoran, 2013). Repairing low and high alloy steels requires high-temperature post-weld heat treatments (PWHT), and in some cases, it is not possible (Klenk, 2003; Budzakova, 2004; Cleiton, 2009).

Due to the problems discussed above, a new method was used in the Ahvaz Pipe Plant for repairing the fin-pass rolls. In this method, the damaged regions of the side rolls were separated by a grinding machine, and two rings of AISI D2 steel (due to its high intrinsic resistance to wear) were mounted between the fin roll and the side rolls. However, after a short time (about one year), damage occurred to the rings, which occasionally resulted in the total fracture of the rings. In the present study, the failure mechanism of the fin-pass rolls was investigated. Finite element simulation was used to study the role of contact stresses on the failure mechanism of the rolls. In addition, alternative materials, namely hard chromium plated AISI 4140 steel, case hardened AISI 4140 steel, and carburized AISI P20 steel, compared with AISI D2 steel were proposed for the rings.

2. Experimental procedures

The fin-pass rollers investigated in this study had three pieces, and their schematic view is shown in Figure 1a. These rollers are used to adjust the contact edges of the pipe prior to welding in the ERW pipe manufacturing line. Its middle part, which has the function of adjusting the edges of the joint, is called the fin roll, and its side parts which form the cross section of the sheets, are called the fin side rolls. The first stage of the repair process was removing the damaged portions of the roll by grinding. Then, it was replaced by two rings with the same geometry made from AISI D2 steel (Figure 1b). The

roller sections might be increased to three or five parts. Their failure mechanism was studied by scanning electron microscopy (SEM), model MV2300, to investigate the performance of fin-pass rollers. In addition, the finite element simulation method was used to perform the stress analysis by ABAQUS 6.14 software. Figure 1c schematically illustrates the forming rolls and the sheet in the finite element simulation model for the ERW pipe manufacturing line studied in the present research. A 3D deformable part was used to define the fin-pass roller and the sheet in this model. Other rollers were defined as rigid parts. The studied fin-pass roller was defined with two geometries containing three and five pieces, schematically shown in Figure 1a and 1b, respectively. The solving method was dynamic explicit.

In the present study, case hardened AISI 4140 steel and carburized low-carbon AISI P20 steel were studied to modify the material selection and improve the wear resistance of repaired rings.
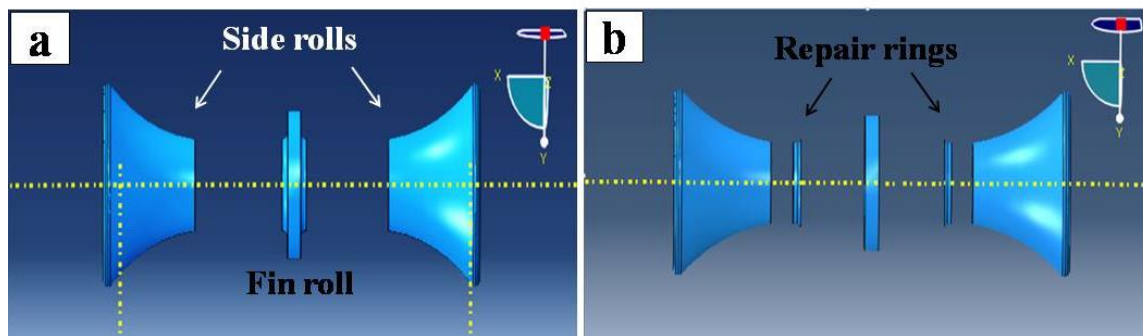

Figure 1
a) A schematic view of the three-piece fin-pass roll and b) a schematic view of the five-piece fin-pass roll.

Carburization of low-carbon AISI P20 steel was carried out by solid pack cementation method at 925 °C for 1 h in a medium containing 78% charcoal, 10% NaOH, and 3% calcium carbonate. After cooling the furnace to ambient temperature, normalization heat treatment was carried out by austenitizing at 850 °C for 1 h and cooling in air to decrease the grain size. In the second stage, austenitizing was carried out at 850 °C for 1 h and then quenching in oil to change the microstructure of the surface to martensite. The case hardening operation of AISI 4140 steel was performed using the induction hardening method with 30 s surface austenitizing and then cooling with a water jet. During induction heating, the surface temperature was measured at 860 °C by a non-contact infra-red thermometer (JXB-178 model).

The chrome plating of the AISI 4140 steel was performed in a plating bath containing 200 g/L chromic acid and 2 g/L H_2SO_4 at 35 °C using a lead anode. The current density of electroplating was 40 A/dm^2. Before electroplating, the case-hardened AISI 4140 steel substrate was first ground with SiC emery papers and then cleaned in an industrial degreasing liquid. Subsequently, the substrate was activated in a solution containing 20% sulfuric acid and 10% hydrochloric acid and washed with water. The plating time was 1 h, and the coating thickness was 60 µm.

Hardness testing of the samples was carried out by the Vickers hardness method using an HXD-10000 apparatus, and the applied force was 60 grams. The pin evaluated the wear resistance of the specimens on the disk wear test. The two-piece specimens were selected to investigate the edge conditions affected by stress and the impact of the counterparts. The dimensions of each piece of the specimen were 15 × 15 × 30 mm^3. The wear test was performed using a flat pin with a diameter of 6 mm and a hardness of 60 Rockwell C made from AISI 52100 steel. The sliding distance was 500 m at a normal force of 10 N and a linear speed of 20 m/min. The friction coefficient of the specimens was measured according to the following equation:

$$W_r = \frac{\Delta m}{d \times F}$$

(1)

where Δm (g) is the mass change of the sample, d (m) indicates the wear distance, F(N) represents the normal force, and W_r(g/N.m) is the friction coefficient. After the wear tests, the worn surfaces were examined by SEM to understand the wear mechanism better.

3. Results and discussion

3.1. The failure analysis

In order to identify the causes of damage to the fin-pass rollers, a detailed visual examination of their surface was performed in the damaged areas. The results are shown in Figure 2. Figure 2a shows a macroscopic image of the fin-pass roller repaired using repair rings after one year of service. The partial signs of wear are visible on the surface of side rolls, which has a minor effect on the performance of the fin-pass rolls and can be neglected. However, it is evident in higher magnification (Figure 2b) that spalling has occurred on the edge of the repair ring, resulting in detrimental effects on the performance of the fin-pass rolls. In addition, the spalled regions could lead to stress concentration and finally result in fracture. For closer investigation, scanning electron microscopy images were taken from the surface of repair rings at the damaged sites to identify the destruction mechanism.
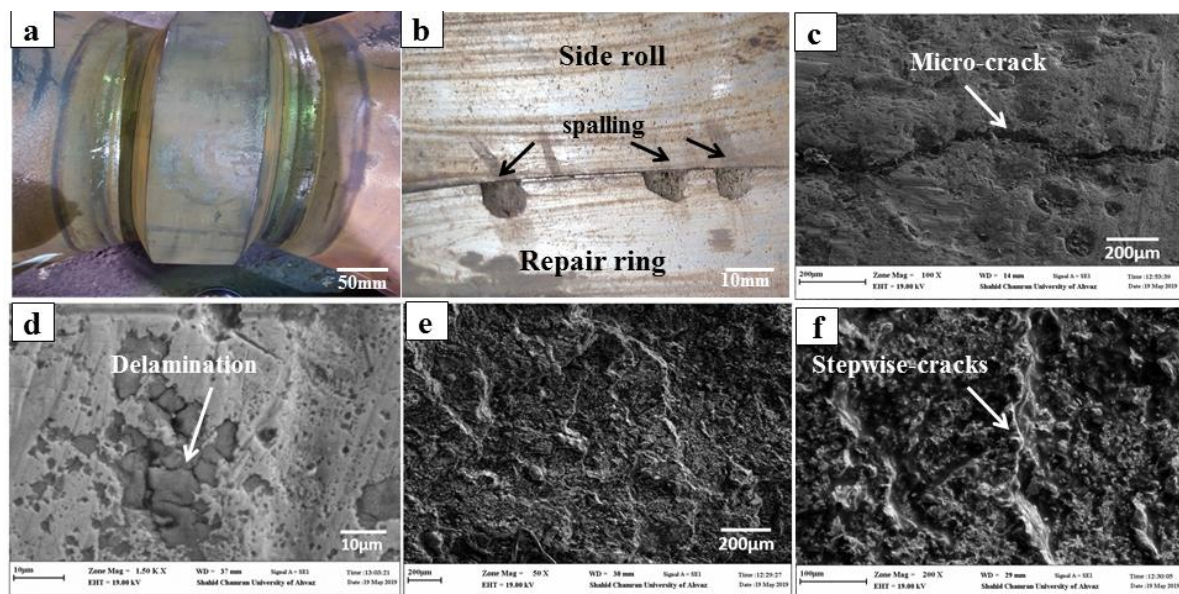

Figure 2

Macroscopic and microscopic images of the damaged surface of the fin-pass roller: a) magnification ×0.1 (optical); b) magnification ×10 (optical); c) electron microscopic image of the not spalled edge regions (SEM); d) electron microscopic image of the dull edge regions with ×500 magnification (SEM); e) the same specimen at ×1000 magnification (SEM); f) Fin-pass roller electron microscopy image in non-edge areas (SEM).

Figure 2c shows the surface morphology of the roller in areas with no spalling signs at ×100 magnification. A surface microcrack is visible. At a higher magnification (×150) (Figure 2d), some minor grooves and soft dull edges can be seen, showing minor delamination and abrasive wear. In the delamination mechanism, cyclic stresses accumulate work hardening beneath the surface, resulting in the initiation and propagation of microcracks from the subsurface regions to the outer surface. In these

conditions, negligible wear is observed indicative of high wear resistance of the repair ring (made from AISI D2 steel), which has no significant effect on the performance of the fin-pass rolls. Figure 2e illustrates the scanning electron micrographs of the spalled area of the repair ring at its edge. In addition, a higher magnification image is shown in Figure 2f, which reveals the signs of the stepwise crack growth pattern, which can indicate that the crack growth occurs by the fatigue mechanism. The collision of the edge of the sheet with the revolving repair ring during the forming process caused cyclic stresses that led to the beginning of fatigue. In addition, stress concentration at the edge of the repair rings can increase the cyclic stress level and intensify the fatigue crack growth. The fatigue cracks probably nucleated from the surface and grew inwards, causing the spalling at the edges of the repair rings (Premsai 2014). The mild surface grooves or delamination-induced slits are prone to stress concentration, initiation, and growth of the fatigue cracks. The negligible effects of wear on the surface of the repair ring are signs of the high wear resistance of AISI D2 steel. However, the occurrence of spalling at its edge in a shorter time than the AISI 8622 steel (original material of the side roll) demonstrates the low fatigue resistance of AISI D2 steel due to the low toughness of the AISI D2 alloy, which results in its spalling and eventually leads to the fracture of the repair ring.

3.2. The finite element analysis of the fin-pass roll

The finite element simulation was performed to investigate the stress analysis of different segments of the fin-pass roll parts in two different conditions, the presence and absence of the repair ring, which can lead to a better understanding of the failure mechanism of the fin-pass roll and thus a better choice of the methods to improve their life. As shown in Figure 1b, the first fin-pass roll under consideration has been designed by the deformable element type. For better observation, its higher magnification image is also illustrated in Figure 3c. Figure 3b demonstrates that the rest of the rolls have been designed using rigid type elements, which is beneficial to further reducing the time and cost of the solution.
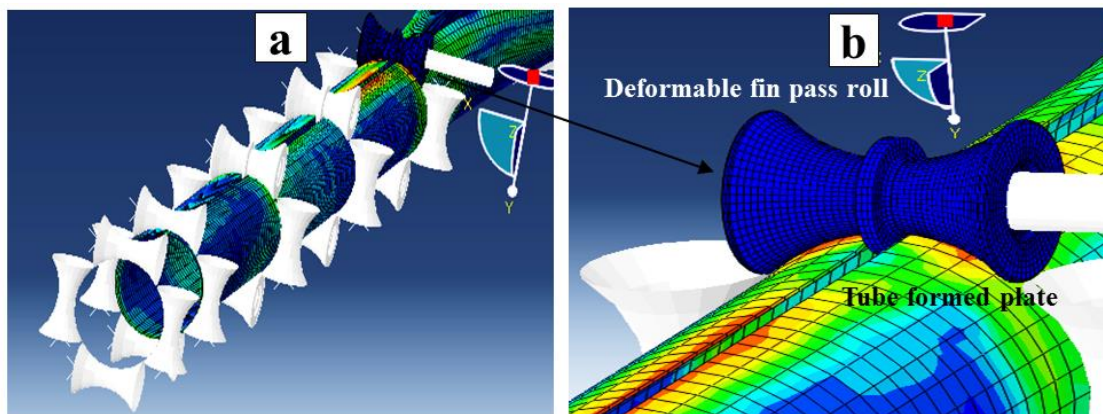

Figure 3
The results of the finite element analysis of Von-Mises stress: a) pulling the tubular formed sheet between the forming rollers; b) the investigated first row fin-pass rollers with a deformable element at a higher magnification.

Figure 4a to 4b shows the Von-Mises stress distribution at different roller components of three and five using the repair rings. For better viewing, the sheet is omitted, and only the first row of the fin-pass roller is shown. Figure 4a shows the Von-Mises stress distribution of the fin-pass roller without repair rings three-piece mode. The maximum Von-Misses stress is 180 MPa in this case. Figure 4b shows the Von-Mises stress distribution of the fin-pass roller with repair rings (five-piece mode). The maximum stress value is 440 MPa, which is significantly higher than the value (180 MPa) at the fin-pass roller without repair rings (Figure 4b). Comparing Figure 4a with 4b shows that increasing the number of

roller components from three to five using the repair rings increases the maximum stress value, especially at the repair ring due to the low width of the ring and the synergy of the interfacial stresses at its edges increasing the mean stress. It indicates that repair rings are further prone to failure and fracture due to higher stress concentration. In this case, the higher values of the stresses will facilitate the initiation and growth of the fatigue cracks and thus shorten the lifetime, which agrees with the observation of spalling in a shorter time at the edges of the repair ring than the edge of the side roll.
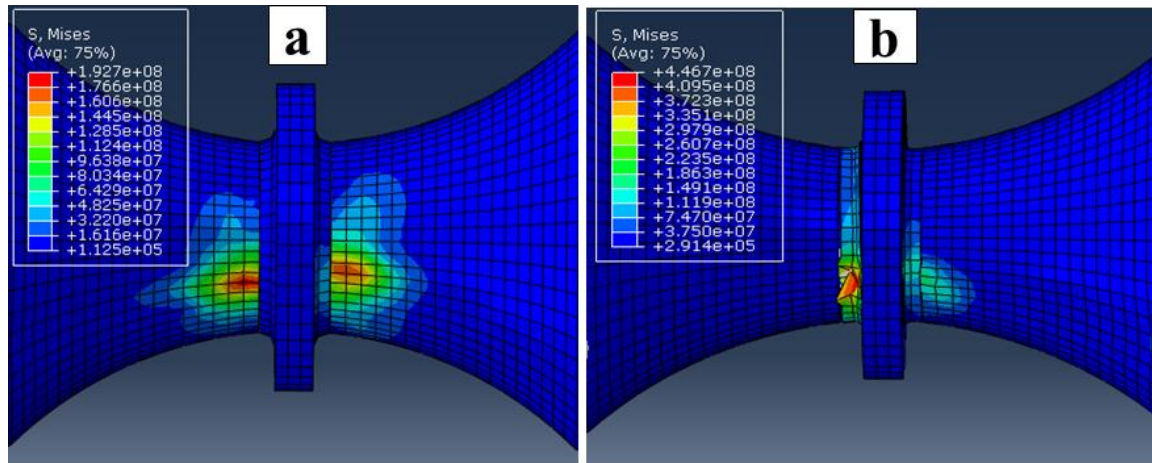

Figure 4
Distribution of Von-Mises stresses for fin-pass roller without repair ring (three-piece roller) at different values of the friction coefficient between its components: a) $W_r = 0$; b) $W_r = 0.5$; c) $W_r = 1$; d) distribution of Von-Mises stresses for fin-pass roller with repair rings (five-piece roller) at values of 0.5 for friction coefficient between its components.

3.3. Modification of the material of the rollers

As mentioned in the failure analysis section, a potential solution to extending the service life of the repair ring is to use an alternative material with higher toughness and to use a suitable surface treatment to achieve higher wear resistance. This study proposed low-carbon AISI P20 steel and medium-carbon AISI 4140 steel alloys with higher toughness than high-carbon AISI D2 steel. For low-carbon steels, surface carburization and medium-carbon steels case hardening and hard chromium plating can be suitable surface treatments to increase the wear resistance. Thus, the carburization of AISI P20 steel, the case hardening, and the hard chromium electroplating operations on AISI 4140 steel were performed. Figure 5a shows the cross-sectional morphology of the case hardened AISI 4140 steel. Further, Figure 5b and 5c shows the microstructure of the near-surface areas and the deeper portions of this specimen at higher magnification, respectively. Observation of martensite blades on the surface of this steel can lead to high surface hardness. In addition, the pearlite-ferrite microstructure in the deeper portions can indicate the high toughness in these areas.
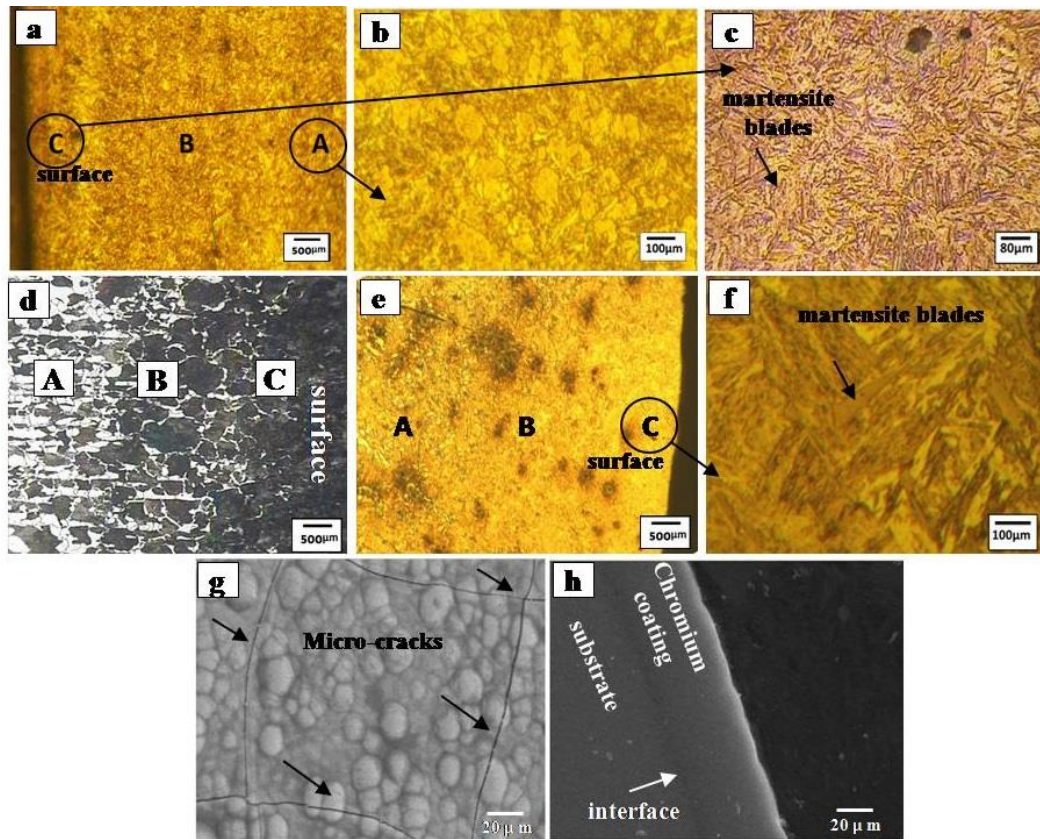
Figure 5
Optical microscopic images of a) the cross-sectional microstructure of case hardened AISI 4140 sample, b) the higher magnification of the surface area in image a, c) the higher magnification of the deeper area at image a, d) the cross-sectional microstructure of carburized P20 steel before quenching, e) the cross-sectional microstructure of carburized AISI P20 steel after quenching, f) the higher magnification of the deeper areas in image e, g) the SEM image of the hard chromium electroplated AISI 4140 sample, and h) the cross-sectional SEM image of the hard chromium electroplated AISI 4140 sample.

Figure 5d shows the light microscope image of the cross section of carbonized AISI P20 steel prior to the quenching operation. It is evident that the surface microstructure is cementite, and with moving inwards, the microstructure changed to ferrite. The presence of ferritic microstructure in the depth of this sample indicates the high toughness in these areas.

Figure 5e illustrates the cross-sectional image of this sample after the quenching operation. In addition, Figure 5f shows the microstructure near the surface regions of this sample at a higher magnification. It is evident that after quenching, the surface microstructure of this sample is martensitic, which can lead to high surface hardness. Figure 5g and 5h shows the scanning electron microscope images of the hard chromium electroplated AISI 4140 steel from its surface and cross section, respectively. The surface morphology in Figure 5g contains many colonies and microcracks, which is similar to the results of previous studies (Fedrizzi, 2002; Lindsay, 1997). The surface colonies are collections of the grains. Observation of the microcracks indicates the high residual stresses in the hard chromium coating. The high residual stresses between the atoms, in this case, will retard the movement of the dislocations and thus increase the hardness [Sun, 2020]. The surface hardness of this specimen was 1200 HV, which is significantly higher than that of its substrate (about 60 Rockwell). Figure 5h shows that the interfacial adhesion between the coating and the substrate is well, and the thickness of the coating is 50 µm approximately. Figures 6 and 7 show the indenter projections of the microhardness tests from the surface toward the depth for case hardened AISI 4140 and carburized AISI P20 steel, respectively.
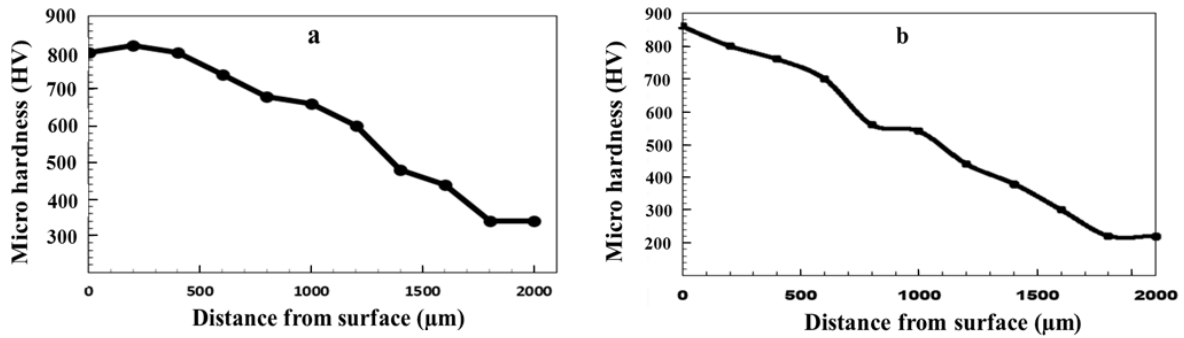
Figure 6
a) The change of microhardness values versus distance from surface for case hardened AISI 4140 steel and b) variation of microhardness values versus the distance from the surface for carburized AISI P20 steel.

In both cases, it is well observed that in areas close to the surface, the dimensions of the indenter projection are small, which indicates high surface hardness. It is clear that with moving from the surface toward the depth, the dimensions of the indenter projection gradually increase, which is the sign of the gradual decrease in the microhardness values. The curves of these variations show that the hardness values are high at the surface and gradually decrease from the surface into the depth. The high surface hardness, in this case, is due to the martensitic microstructure and the decrease in hardness in the inner portions is due to the change of microstructure to the ferritic-pearlitic one. It is also clear that the surface hardness of the carburized AISI P20 steel is greater than that of the case hardened AISI 4140 steel due to the higher carbon content at the surface of carbonized AISI P20 steel. Previous studies showed that increasing the carbon concentration increases the hardness of the martensite microstructure (Clarke, 2008). Since the super-saturation level in the crystal lattice increases, the internal stresses increase, which implies moving the dislocations is more complicated. In this case, the higher surface hardness can lead to the higher wear resistance of AISI P20 steel. It is also evident that the hardness in the bulk of the carburized AISI P20 steel is less than that of the case hardened AISI 4140 steel due to the lower carbon content in the bulk of AISI P20 steel than that of AISI 4140 steel. The lower hardness, in this case, can lead to higher toughness in AISI P20 steel.
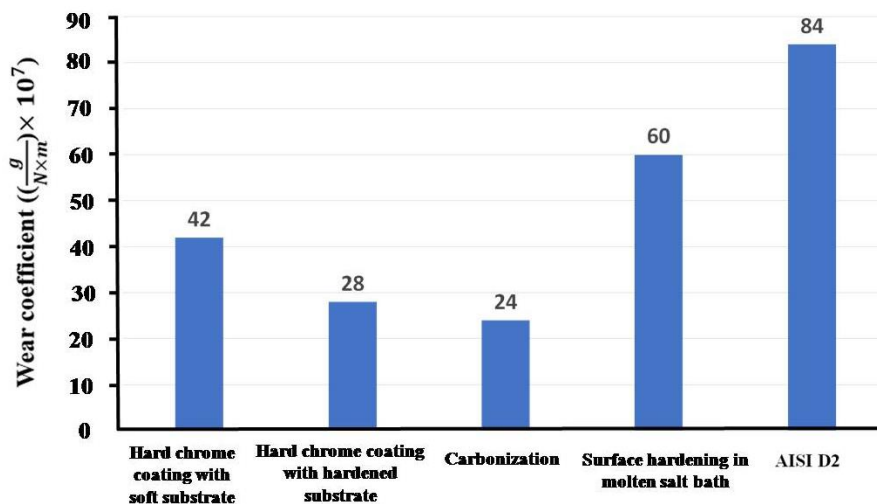

Figure 7
Wear coefficient of the various steel samples.

Figure 7 shows the wear coefficient of the hard chromium electroplated AISI 4140 steel, case hardened AISI 4140, and carburized AISI P20 and AISI D2 steel. Moreover, for a better understanding of the

wear mechanism, the SEM images of the worn surfaces of these samples are shown in Figure 8. As shown in Figure 7, the wear rate of the carburized AISI P20 sample is lower than the other samples, which indicates the better wear resistance of this sample. At the subsequent levels, the hard chromium electroplated AISI 4140 steel the case hardened AISI 4140 sample has the following low wear rates. The highest wear rate is for the AISI D2 steel specimen. For a better interpretation of the wear mechanism of the different specimens, the worn surface of the specimens was examined using scanning electron microscopy in Figure 8 at different magnifications.
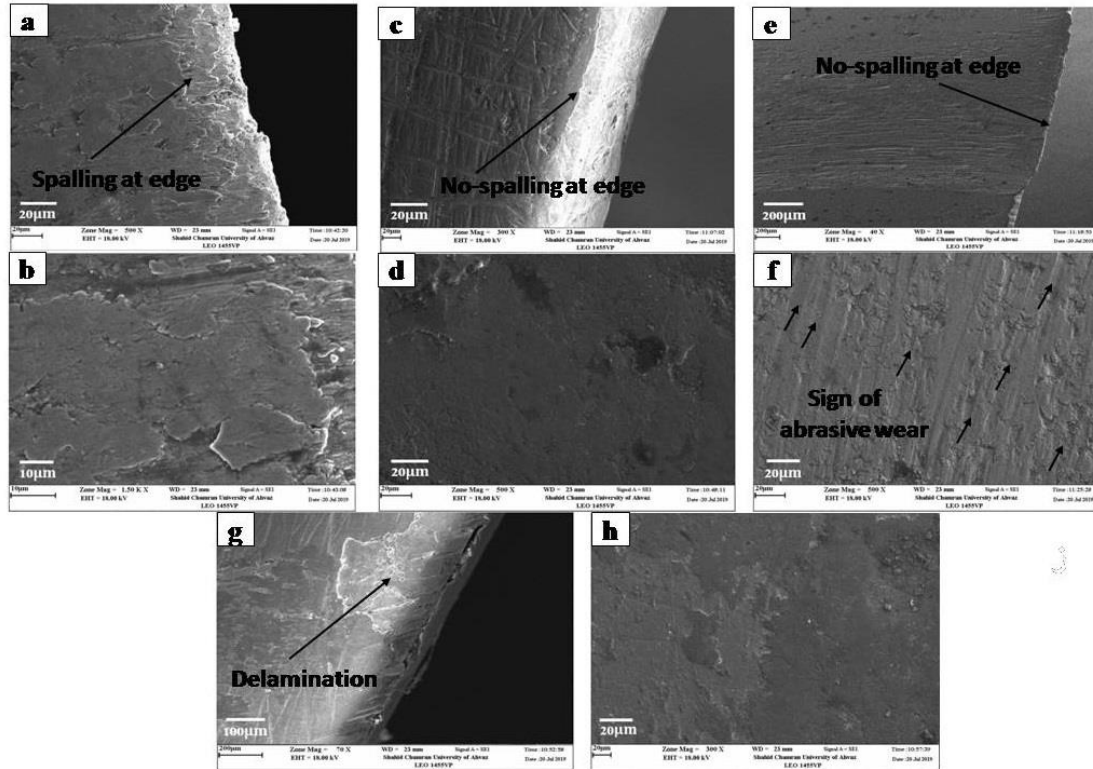

Figure 8
Scanning electron microscopy images of a) the edge of the wear test specimens of AISI D2 steel, b) the worn surface of AISI D2 steel, c) the edge of the carburized AISI P20 specimens, d) the worn surface of the carburized AISI P20 steel, e) the edge of the wear test specimens of the case hardened AISI 4140 steel, f) the worn surface of the case hardened AISI 4140 steel, g) the edge of the wear test specimens of the hard chromium electroplated AISI 4140 steel, h) the worn surface of the hard chromium electroplated AISI 4140 steel.

According to Figure 8a, spalling occurred at the edge of AISI D2 steel due to the inherent low toughness of this steel that cannot withstand the stress concentration of the wear test. In addition, the mild effects of wear at higher magnifications can be seen (Figure 8b). Observation of the highest wear rate for this specimen can be attributed to the occurrence of spalling that causes significant weight loss. Figure 8c shows the worn surface of the edge of the carburized AISI P20 wears test specimen. No spalling has taken place. The reason is the gradual increase in toughness from the surface to the depth of this specimen due to the gradual change of the microstructure from martensitic to pearlitic–ferritic one. In this case, with a gradual increase in toughness from the surface to the depth, the specimen becomes more resistant to the growing microcracks (Cavaliere, 2008; Savrai, 2021). In addition, according to Figure 8d, the worn surface of this specimen is very smooth, which is in agreement with the observation of the highest wear resistance for this specimen than the others. The smoothness of the worn surface indicates that the specimen could overcome the sliding wear mechanism, and adhesive and abrasive

wear are not significant due to the high hardness of the martensitic microstructure and the high carbon concentration of the surface layers, leading to high wear resistance (Hotz, 2020).

Figure 8e and 8f shows the worn surface images at the edge and surface of the case hardened AISI 4140 steel, respectively. No spalling could be seen at the edge of the specimen. However, signs of abrasive wear are noticeable on the surface of the sample related to the lower hardness of this specimen than the carburized AISI P20 steel. Figure 8g and 8h shows the worn surfaces at the edge and surface of the hard chromium electroplated AISI 4140 steel, respectively. No spalling happened on the edge of the test specimen. However, some delaminating of hard chromium coating is observable, which may be related to the high residual stresses of the hard chromium coating, which are accompanied by high values of stress concentration at the edges and led to the removal of the coating. The high internal stress of the hard chromium coatings is related to the stresses encountered during the electroplating process. The high current density causes the atoms not to be in equilibrium during electroplating, leading to high internal stresses (Andrew, 2021; Pfeiffer, 2011). However, the worn surface of this specimen is smooth, and there are negligible effects of severe abrasive and adhesive wear, which agrees with observing good wear resistance for this sample after the carburized AISI P20 steel specimen.

According to the results of the wear tests, the carburized AISI P20 sample showed the highest wear resistance compared to the other specimens. Therefore, manufacturing the repair rings from AISI P20 steel and carburizing its surface are an excellent solution to improving its service life, which can improve the performance of the fin-pass rollers after the repairing process.

4. Conclusions

The leading failure cause of the AISI D2 steel repair ring in renovated fin-pass rolls was the spalling of the phenomenon at the edge, which occurred by the fatigue mechanism. Using finite element simulation, it was observed that the use of repair rings for repaired damped fin-pass rolls causes severe stress concentration in the repair rings, identified as the leading cause of the rapid destruction of the repair rings. The results showed that using tougher steel such as P20 steel and its surface hardening by carbonization method could improve the resistance to the spalling phenomenon and the excellent wear resistance.

Nomenclature

ERW	Electric resistance welding
PWHT	Post-weld heat treatments
SEM	Scanning electron microscopy

Acknowledgments

References

Budzakova, E., Dune, D., Law, M., The Performance of an Emergency Cold Weld Repair on A 2.25Cr-1Mo Longitudinally Seam Welded Pressure Vessel, Mater. Forum, Vol.27, p.45–53,2004.

Cavaliere, P., Crack Tip Plasticity in Plastically Graded Ni–W Electrodeposited Nanocrystalline Alloys, Comput. Mater. Sci. Vol.41–4, p.440–449, 2008, DOI:10.1016/J.Commatsci.2007.05.007.

Christopher, A., Luzin, A.V., Travis, S., Howard, G., Andrew, A., And A Mechanical Performance and Residual Stress of WC-Co Coatings Manufactured by Kinetic Metallization, Surface and Coatings Technology, Vol.421, p.27–35,2021.

Clarke, AJ., Speer, JG., Miller, MK., Hackenberg, RE., Edmonds, DV., Matlock, DK., Rizzo, C., Clarke, KD., Moorf, ED., Carbon Partitioning To Austenite From Martensite Or Bainite During The Quench and Partition (Q&P) Process. Acta Mater. Vol.56, No.1, p.16–22, 2008, DOI:10.1016/J.Actamat.2007.08.051.

Cleiton, CS., Victor, HC., Cícero, DA., Moura, RO., Aguiar, WM., Jesualdo PF Evaluation of AISI 4140 Steel Repair without Post-weld Heat Treatment. J. Mater. Eng. Perform, Vol.18, p.324–331, 2009,DOI: 10.1007/S11665-008-9294-5.

Fedrizzi, L., Rossi, S., Bellei, F., Deflorian, F., Wear-corrosion Mechanism of Hard Chromium Coatings, Wear, Vol.253,p.173–1181, 2002, DOI:10.1016/S0043-1648(02)00254-5.

Hotz, H., Kirsch, B., Zhu, T., Smaga, M., Beck, T., Jan, C. Surface Layer Hardening of Metastable Austenitic Steel – Comparison of Shot Peening and Cryogenic Turning, Journal of Materials Research and Technology, 2020, Vol.9, p.16410–16422. Https://Doi.Org/10.1016/J.Jmrt.2020.11.109.

Jiang, J., Li, D., Peng, Y., Li, J., Research on Sheet Deformation in The Cage Roll-forming Process of ERW Round Pipes. J. Mater, Process, Technol, 2009, Vol.209p.4850–4856, DOI:10.1016/J.Jmatprotec.2009.01.011.

Kasaei, MM., Naeini, HM., Tafti, RA., Tehrani, MS., Prediction of Maximum Initial Strip Width in The Cage Roll Forming Process of ERW Pipes Using Edge Buckling Criterion. J. Mater. Process. Technol. Vol.214, No.2, p.190–199. 2014, DOI:10.1016/J.Jmatprotec.2013.08.012.

Kim, N., Kang, B., Lee. S., Prediction and Design of Edge Shape of Initial Sheet for Thick Tube Roll Forming Using Finite Element Method, J. Mater. Process. Technol, Vol.142, p.479–486, 2003,DOI:10.1016/S0924-0136(03)00645-9.

Kiuchi, M., Optimum Design of Fin-rolls and Fin Pass-schedule of Roll Forming of Pipes, Proceedings of Tomorrow Tube-international Conference and Exposition, Birmingham, England, p.459–479, 1986.

Klenk, S., Issler, IA., Shibli, J., Williams, A., Some Characteristics of Weld Repair for Creep Applications, OMMI. Vol.2, p.1–32, 2003.

Li, H., Jiang, Z., Tieu, KA., Sun, W., Analysis Of Premature Failure of Work Rolls in A Cold Strip Plant. Wear, Vol. 263, p.1442–1446, 2007, DOI:10.1016/J.Wear.2007.01.126.

Li, JX., Xie, LY., Wang, JJ., Xiong, JH., Numerical Study of The Forming Process of High-Frequency Welded, Pipe J., Shanghai Jiaotong University, Vol.15, p.236–240, 2010, DOI:10.1007/S12204-010-8131-9.

Lindsay, JH., Decorative and Hard Chromium Plating. Plat. Surf. Finish, Vol.84–8, p.50–51,1997.

Michitoshi, T., Isamu, K., Osamu, S., Outline of New Forming Equipment for Hikari 24__ ERW Mill, Nippon Steel Technical Report, Vol.90, p.122–126,2004.

Paralikas, J., Salonitis, K., Chryssolouris, G., Investigation of The Effect of Roll Forming Pass Design on Main Redundant Deformations on Profiles from AHSS, Int. J. Adv. Manuf. Technol., Vol.56, p.475–491, 2011, DOI:10.1007/S00170-011-3208-7.

Pfeiffer, W., Koplin, C., Reisacher, E., Wenzel JResidual Stresses and Strength of Hard Chromium Coatings, Materials Science, Vol.681, p.133–138, 2011, DOI: 10.4028/Www.Scientific.Net/MSF.681.133.

Premsai, T., Varma, AKV., Sivarajan, S., Failure Analysis Of Rollers In Mill Stand Using Failure Mode Effect Analysis. Int. J. Eng. Sci. Res. Technol, Vol.3, No.7,p.151–159,2014.

Ray, AK., Mishra, KK., Das, G., Chaudhary, PN., Life of Rolls in A Cold Rolling Mill in A Steel Plant Operation Versus Manufacture, Eng. Fail. Anal, Vol.7, p.65–67,2000,DOI:10.1016/S1350-6307(99)00004-7 .

Savrai, RA., Osintseva AL Effect Of Hardened Surface Layer Obtained by Frictional Treatment on The Contact Endurance of The AISI 321 Stainless Steel Under Contact Gigacycle Fatigue Tests, Materials Science and Engineering: A, Vol.802, p. 140–169, 2021, Https://Doi.Org/10.1016/J.Msea, 2020,140679.

Sunabc, Y.L., Hamelincda, J., Vasileioueq, N., Xiongat, F., Flintag Ob asifj. A. Francisam C. Smith Effects of Dilution on The Hardness and Residual Stresses in Multipass Steel Weldments International Journal of Pressure Vessels and Piping, Vol.187, p.104–154, 2020.

Tanasković, D., Đorđević, B., Tatić, U., Sedmak, S., Gajin, M., Cracking Due to Repair Welding of The Treiber Roll. Struct. Integrity Life, Vol.17, No.2, p.133–138,2017.

Wang, X., Wang, J., Gao, Z., Xia, DH., Hu, W., Fabrication of Graded Surfacing Layer for The Repair of Failed H13 Mandrel Using Submerged Arc Welding Technology, J. Mater. Process. Technol., Vol.262, p.182–188, 2018, DOI:10.1016/J.Jmatprotec,2018.06.040.

William, E. B., Pipeline Planning and Construction Field Manual, Elsevier Inc, Chapter 3, p.57–65,2011.

Wu, Q., Sun, DL., Liu, CS., Li, CG. Analysis of Surface and Sub-surface Initiated Spalling of Forged Cold Work Rolls Eng. Fail. Anal., Vol. 14, p.401–410, 2008, DOI:10.1016/J.Engfailanal.2007.01.009.

Yokoyama, E., Toyooka, T., Ejima, A., Yoshimoto, Y., Kawate, T., Kumata, K., Steel Sheet Deformation Behavior and Forming Load Determination in The 26-Inch Cage Forming ERW Pipe Mill. Kawasaki Steel Technical Report, Vol. 4, p.72–83,1981.

Zoran, O., Miodrag, A., Vencislav, G., Mile, D., Investigation of The Repair Welding Technology Using Ni Base Electrode, Adv. Mater. Res. Vol.814, p.25–32, 2013, DOI:10.4028/Www.Scientific.Net/AMR.814.25.